FLOW STRUCTURES AROUND A CONSTANT-RATE PITCHING AIRFOIL AND MECHANISM OF DYNAMIC STALL [①]

M. Sun, J.L. Wang and Q.X. Lian
Beijing University of Aeronautics and Astronautics

ABSTRACT

The vortical flow structure of a constant-rate pitching airfoil is studied numerically and by flow visualization method. N–S equation in vorticity–stream function form is solved using ADI method for the vorticity equation and a direct method for the stream–function equation. Hydrogen bubble technique is used for flow visualization. The time development of the separated ftow structure on the upper surface of the airfoil and the structure of vortex sheet shed from lower surface boundary layer at the trailing edge are revealed, and effects of pitch rate and pitch axis location are studied. Based on the vortical flow structures and calculated aerodynamic forces on the airfoil, and using vorticity dynamics theory, the mechanism of dynamic stall is stadied and insights are provided.

I. INTRODUCTION

One of the most complex and interesting flow phenomena in unsteady aerodynamics is the delay of boundary layer separation and formation of vortices on a lifting surface undergoing pitching motions, or dynamic stall. The majority of the research on dynamic stall has been concentrated on airfoils subjected to sinusoidal pitching oscillations, motivated by its application to helicopter blade stall[1]. Progress in this problem area is hindered by the need to account for many interrelated flow parameters. In addition to the usual flow field dependance on Reynolds number, Mach number and airfoil shape, the effects of mean angle of attack, frequency and amplitude of the forcing motion must be considered. Recently much work has been done on the case of constant–rate pitching motion[1,2]. Interest in this problem have been stimulated by projected aircraft manoeuvrability enhancement. The study of constant–rate pitching, starting from a well defined steady flow condition, is also attractive because it allows the investigation of dynamic stall without the added complexity of motion history effects.

Based on the theoretical work of Wu[3] it can be shown that for imcompressible flow the force exerted by the fluid on the airfoil is dominated by the time rate of change of the first moment of vorticity in the flow field. Therefore, it is interesting to know the vortical flow structures of the airfoil, their evolution with time, and the effects of pitching rate and other parameters, in order to understand the mechanism of dynamic stall. In previous experiments on flow visualization for constant–rate pitching airfoil, markers were introduced into the flow field from the upstream of the airfoil and flowed into the large–scale vortical system. Detailed flow structures were not observed. Recent numerical studies[1,2] revealed complex separated flow structures on the upper surface of the airfoil. But in these studies, consideration was not given to the vortex sheet shed into the wake from the lower surface boundary layer at the trailing edge, and the mechanisms of generation of high lift and dynamic stall were not well explained. In this paper, the separated flow structure and the structure of the vortex sheet in the wake of a constant–rate pitching airfoil are investigated numerically and by flow visualization method, and based on the flow structures and calculated aerodynamic forces on the airfoil, and using the theory of vorticity dynamics, the mechanism of dynamic stall is studied.

II. Governing Equations, Boundary Conditions, and Numerical Procedure

In the rotating reference frame in fig. 1, vorticity equation and stream–function equation are

$$\omega_t + \psi_y \omega_x - \psi_x \omega_y = \frac{1}{R_{e,l}}(\omega_{xx} + \omega_{yy})$$
$$- 2\frac{d\Omega}{dt} \tag{1}$$

$$\psi_{xx} + \psi_{yy} = -\omega \tag{2}$$

where ω is the vorticity, ψ the stream function and Ω the pitch rate, and variables in the above equations have been nondimensionalized using l, u_∞, and $1/u_\infty$ as the reference length, velocity and time respectively (u_∞ is the free stream speed and $l = c/\lambda$, where c is the chord length of the airfoil and λ is a constant). $Re.l = lu_\infty/\nu = Re/\lambda$ and $\Omega = 2\Omega^*/\lambda$ (Re is chord Reynolds number and Ω^* the nondimensional pitch rate using $c/2$ as reference length). The vorticity and stream function in inertial frame of reference, ω_I and ψ_I, can be related to ω and ψ as

$$\omega_I = \omega + 2\Omega \tag{3}$$

$$\psi_I = \psi - \Omega(x^2 + y^2)/2 \tag{4}$$

For generation of computational grid,

$$z = z_1 + \gamma + b^2/(z_1 + \gamma) - \sigma \tag{5}$$

is used to map an unit circle in $z_1 = re^{i\theta}$ plane onto an airfoil of chord length λ in z plane, and with $b^2 = 0.7608954$ and $\gamma = -0.0769384$, equation (5) closely defined a NACA0015 airfoil in z plane. Furthermore, letting

$$r = exp(\pi\xi), \quad \theta = \pi\eta \tag{6}$$

equation (5) maps a rectangular domain with uniform grid in $\zeta = \xi + i\eta$ plane onto a domain in z plane with close grid nodes near the airfoil, fig.1. In ζ plane equation (3) and (4) become

$$\left|\frac{dz}{d\zeta}\right|^2 \omega_t + (\psi_\eta\omega)_\xi - (\psi_\xi\omega)_\eta = \frac{1}{Re,l}(\omega_{\xi\xi}$$
$$+ \omega_{\eta\eta}) - 2\left|\frac{dz}{d\zeta}\right|^2 \frac{d\Omega}{dt} \tag{7}$$

$$\psi_{\xi\xi} + \psi_{\eta\eta} = -\left|\frac{dz}{d\zeta}\right|^2 \omega \tag{8}$$

The boundary conditions are prescribed as follows:

$$\psi = 0, \quad \omega = -\psi_{\xi\xi}/\left|\frac{dz}{d\zeta}\right|^2, \quad at \ \xi = 0, \ 0 \leqslant \eta$$
$$\leqslant 2, \ t > 0 \tag{9}$$

$$\psi = \psi_{I,0} + \Omega(x^2 + y^2)/2, \quad \omega = \omega_{I,0}$$
$$- 2\Omega, \quad at \ \xi = \xi_0, \ 0 \leqslant \eta \leqslant 2, \ t > 0 \tag{10}$$

where $\psi_{I,0}$ and $\omega_{I,0}$ are the stream function and vorticity on the for field boundary (seeing from the inertial frame of reference), which are approximated by the potential flow solution of the airfoil.

$$\psi_{I,0} = 2sh\pi\xi_0 sin[\pi\eta - \alpha(t)] \tag{11}$$

$$\omega_{I,0} = 0 \tag{12}$$

where α is the angle of attack of the airfoil, fig.1. In this study, the airfoil was first started abruptly at zero angle of attack and after the flow developed for some time, it began to pitch up. Therefore, the initial condition is given by the potential flow solution of the airfoil at zero angle of attack. The surface pressure distribution is obtained by integrating the tangential component of N–S equations in primitive variables and from the pressure distribution the forces are calculated.

Details of the numerical procedure is given in ref.5. The vorticity equation was solved by ADI method. The convection terms were discretized by central differencing scheme and nonlinear terms were lagged a full time step. Surface vorticity was discretized by Wood's second order formula[4]. The total order of accuracy of the method is $O(\Delta\xi^2, \Delta\eta^2, \Delta t)$. The stream function equation was solved by a direct method for Poisson equation (FFT method).

In most of the calculated cases, the chord Reynolds number, pitch axis location and pitch rate were the same as that in the experiment described in next section. Some calcalations were done for different pitch axis locations.

In the calculations, numerical uncertainties were mainly associated with the far field boundary location, spatial resolution, and time step value. Calculations were performed with $\Omega^+ = 0.24$, using $r_0 = 15$, 23 and 30. Difference between the calculated flow structures and forces for $r_0 = 23$ and 30 was small, and correspondence between the calculated flow structures and the flow visualization data was satisfactory. Therefore the far field boundary was put at $r_0 = 23$ in the present study. similar numerical experiments were conducted[5] to determine the grid size, the grid size (200 × 128) was considered suitable for the present study. Numerical experiment[5] also showed that as $\Delta t < 0.001$, numerical solution was effectively independent of time step value. Thenefore $\Delta t = 0.001$ was used in the calculations.

III. Description of Experiment

The experiment was conductad on a NACA 0015 airfoil of 0.1m chord length in a $0.4 \times 0.4 \times$

6.8m^{3}water channel at a chord Reynolds number of 8600 in a wide range of Ω^+ ($\Omega^+ = 0.063$, 0.14, 0.24, 0.36, 0.45, 0.52, 0.64, 0.84, 1.2). The pitch axis location was at 30 % chord position. Hydrogen bubble technique was used in the experiment. Hydrogen bubble wire was arranged in three different ways, fig.2, 1) in the upstream of the airfoil to visualize the overall flow field, 2) near the upper surface of the airfoil to visualize the separated shear layer, 3) at the trailing edge (moving with the airfoil) to visualize the vortex sheet shed into the wake from the lower surface boundary loyer.

IV. Results and Discussion

1. Separated flow structure

Comparison between the calculated and visualized flow pattern showed that the correspondence was satisfactory, but the numerical solution gave more detailed structures of the flow. As an example, fig.3 gives some flow visualization pictures together with numerical solutions (more complete flow visualization data are given in ref. 5).

The time development of streamline pattern from numerical solution for the case of $\Omega^+ = 0.24$ and $x_0 / c = 0.3$ (x_0 is the distance from leading edge to pitch axis) is shown in fig.4, which is used to describe the main features of the upper surface separated flow structure. At $\alpha = 0°$, the flow is symmetric and displays a small reverse flow region near the trailing edge. As the pitching motion begins, the reverse flow at the lower surface dispears, while on the upper surface, the reverse flow region expands upstream. As α is about $30°$, the reverse flow has reached the leading edge of the airfoil, fig. 4a, and there is a shear layer with clockwise vorticity floating on the reverse flow, fig. 4b. The shear layer, resembling a free shear layer, is not stable and after a short time, reorganizes itself into a series of vortices, fig. 4c. In this paper, the vortex near the leading edge is refered as to dynamic stall vortex, and other vortices as to shear layer vortices. There are also some very small secondary vortices below the dynamic stall vortex and shear layer vortices, fig. 4c. The dynamic stall vortex is strong and grows fast in size, fed by the vortex sheet from the leading edge of the airfoil, fig. 4d. As α further increasing, the dynamic vortex absorbs the shear layer vortices into itself while keeps fed by the vortex sheet from the leading edge, fig. 4e, and it becomes larger and larger in size. Finally the dynamic stall vortex begins to move downstream, fig.4f.

For $0.063 < \Omega^+ < 0.52$ ($x_0 / c = 0.3$) in the present study, the upper surface flow development of the airfoil was characterized by the flow features described above, which includes reverse flow region expanding from trailing edge to leading edge, shear layer floating on the reverse flow rolling up into dynamic stall vortex and shear layer vortices, the interaction between these vortices and dynamic vortex dominating the separated flow field, and dynamic stall vortex moving downstream.

The main effect of Ω^+ is that as Ω^+ is increased, the above flow features are delayed, the separated flow region becomes smaller in size and more closed to airfoil surface. For larger Ω^+, only very small dynamic stall vortex forms at very high α and the flow is effectively attached. Fig.5 shows the calculated flow patterns at $\alpha = 45°$ for various Ω^+.

Calculated flow patterns with different pitch axis locations for $\Omega^+ = 0.24$ are show in figs.6 and 7. It is seen that as x_0 / c is increased, the development of dynamic stall vortex is delayed and separated flow region become smaller in size.

2. Vortex sheet shed at the trailing edge

As will be discussed in next section, vorticity shed into the wake from lower surface boundary layer at the trailing edge plays an important role in generating aerodynamic forces on the airfoil. Much less attention was paid to it in previous works. The present flow visualization and numerical studies show that when Ω^+ is relatively small, the vortex sheet is not strong and rolls up into a series of small vortices while convecting downstreum, as is shown in the picture in fig.8a. When Ω^+ is large, the vortex sheet is strong and rolls up into a concentrated vortex near the airfoil, called starting vortex in this paper, as is shown in the picture in fig.8b. Comparison between calculated and flow visualization results for the structure of vortex sheet shed at the trailing edge is good near the airfoil, and the calculated vortices in the wake looks more diffused when they are about one chord length away from the ailfoil. The trajectories of the wake vortices, sketched from flow visualization pictures, for $\Omega^+ = 0.14$ and 0.24, are shown in fig.9. For larger Ω^+, the vortex sheet rolls up into starting vortex and its locations can be measured from the flow pictures, as shown in fig.10. It is interesting to note that for giving α, the vortex is more closed to the airfoil as Ω^+ is increased.

3. Calculated Forces and mechanism of dy-

namic stall

Theoretical analysis of Wu[3] showed that the fore, $\mathbb{F}$, exerted by the fluid on the airfoil could be written as

$$\mathbb{F} = -\rho\frac{d\alpha}{dt} + \rho\frac{d}{dt}\int_A V dA \qquad (13)$$

where ρ is the fluid density, α the first moment of the vorticity in the solid body and the fluid, A the area of the airfoil and V the velocity of some point in A. For constant–rate pitching, it can be shown that both the second term in the right hand side of eg.(13) and the contribution of the vorticity in the rotating solid body to the first term in the right hand side of eq.(13) are proportional to $(\Omega^+)^2(A/c^2)(r_m/c)$, where r_m denotes the distance from the pitching axis to the centroid of A. They are not significant for cases of $\Omega^+ < 1$ (A/c^2, r_m/c are usually much smaller than one). Therefore, the force on the airfoil is mainly from the time rate of change of the first moment of vorticity in the fluid.

Fig.11 shows the calculated aerodynamic force coefficients V.S. α for different Ω^+($x_0/c = 0.3$). It is seen that compared with static case, the lift is increased and stall delayed. When the airfoil is pitching, clockwise vorticity from the upper surface boundary layer remains in the vicinity of the airfoil due to the delay of boundary layer separation and the formation of the dynamic stall vortex and shear layer vortex as discussed above, while counterclockwise vorticity is shed into the wake from the lower boundary layer at trailing edge and convects relatively fast downstream, resulting large time rate of change of first moment of vorticity. This explains, on a qualitative basis, the mechanism of generation of large aerodynamic loads on pitching airfoils. When the dynamic vortex grows large and vorticity in it moves downstream, large time rate of change of first moment of vorticity, with opposite sense to that resulted from counterclock – wise vorticity in the wake, will occur, hence the total time rate of change of first moment of vorticity in the fluid will decrease, resulting lift stall.

For given α, C_L increases as Ω^+ is increased, fig.11. When Ω^+ is increased, because the flow speed on the edge of boundary layer at the trailing edge, denoted by u_L, increases (this can be seen from calculated streamline patterns near the trailing edge, fig.5, and hydrogen bubble time line for cases of hydrogen bubble wire mounted at the trailing edge), the counterclockwise vorticity shed into the wake in

unit time, which is proportional to u_L^2, is increased, and these vorticity usually moves downstream relatively fast, while the separated shear layer on the upper surface become more closed to the airfoil (fig.5), i.e. with less downstream motion. This results in large time rate of change of first moment of vorticity, hence. larger lift.

For $0.063 < \Omega^+ < 0.24$ in fig.11, as Ω^+ increases, lift stall is delayed, which corresponds to the delay of the formation of dynamic stall vortex and its leaving the airfoil as discussed above. It is interesting to note from fig.11 that for $\Omega^+ = 0.52$ and 0.64, the "lift stall" occurs at smaller α (about 30°). At the above conditions, there are not flow separations on the upper surface, fig.5, and the "lift stall" is not in the usual sense. This phenomenon may be explained as following. When Ω^+ is high, the vortex sheet shed at trailing edge rolls up into a concentrated vortex and downstream motion of the shed vortex sheet is slowed and part of the vorticity even moves back towards the airfoil, due to the rolling–up, as seen in fig.8b, resulting in a decrease of the time rate of change of first moment of vorticity.

Fig.12 shows force coefficient V.S. α for various x_0/c ($\Omega^+ = 0.24$). It is seen that as pitch axis moves forward, C_L increases. But from figs.6 and 7, separation occurs earlier and separation region is larger as x_0/c is decreased. Therefore, smaller separation region does not always correspond to larger lift. As x_0/c is decreased for fixed Ω^+, u_L will increase, as can be seen from the streamline plot in figs.6 and 7, and vorticity shed into the wake from lower boundary layer at the trailing edge in unit time will increase. This may result in larger time rate of change of the first moment of vorticity, causing lift to increase.

V. Summary

1) As the airfoil is pitching, starting from $\alpha = 0$, reverse flow region on the upper surface expands from trailing edge to leading edge. The shear layer above the rear flow, resembling a free shear layer, rolles up into shear layer vortices and dyamic stall vortex. The dynamic stall vortex grows fast and dominates the separated flow field.

As Ω^+ is increased, for fixed pitch axis ($x_0/c = 0.30$), or as x_0/c is increased, for fixed Ω^+ ($\Omega^+ = 0.24$), formation of shear layer vortices and dynamic stall vortex will be delayed and separated flow region become smaller in size and more

closed to the airfoil upper surfaee.

2) For $\Omega^+=0.063-0.24$, the vorticity shed from the lower boundary layer at the trailing edge forms a series of small vorteced and convect downstream. For $\Omega^+ > 0.45$, the shed vorticity rolles up into a concentrated vortex and part of the vorticity moves downstream first and then moves towards the airfoil due to the rolling—up.

3) Downstream movement of counterclockwise vorticity shed at the trailing edge, and clockwise vorticity remaining near the airfoil due to delay of separation and formation of shear layer vortices and dynamic vortex, are the mechanism for pitching airfoil generating large lift.

4) For fixed pitch axis $(x_0 / c = 0.3)$, as Ω^+ is increased, more counterclockwise vorticity is shed into wake in unit time, separated region on the upper surface become smaller and closed to the airfoil, and C_L increases.

For fixed $\Omega^+ (\Omega^+ = 0.24)$, as x_0 / c is decreased, more counterclockwise vorticity is shed into wake in unit time, separated region on the upper surface become larger, and C_L increases.

5) When dynamic stall vortex grows larger and vorticity in it moves downstream, causing the total time rate of change of first moment of vorticity to decrease, lift stall occurs. For large $\Omega^+ (\Omega^+ > 0.52)$, boundary layer on upper surface does not separate, but the downstream movement of vortex sheet shed from the trailing edge is slowed and part of the vortex sheet moves towards the airfoil because of the rolling —up of the vortex sheet, resulting in a new type of lift stall.

References

1. Carr, L.W., "Progress in Analysis and Predition of dynamic Stall," J. of Aircraft, 25, 1 (1988), pp. 6–17.

2. Visbal, M.R. and Shang, J.S., "Investigation of the Flow Structure Around a Rapidly Pitching Airfoil," AIAA J. 27, 8 (1989), pp. 1044–1051.

3. Wu, J.C., "Theory for Aerodynamic Force and Moment in Viscous Flows," AIAA J. 19,4 (1981), pp. 432–441.

4. Roache, P.J.,"Computational Fluid Dynamics", 1976, Hermosa Publishers.

5. Wang, J.L., "A Experimental and Computational study of the flow around a constant—Rate Pitching Airfoil", Ph.D Thesis, Beijing University of Aeronautics and Astronautics, 1992.4.
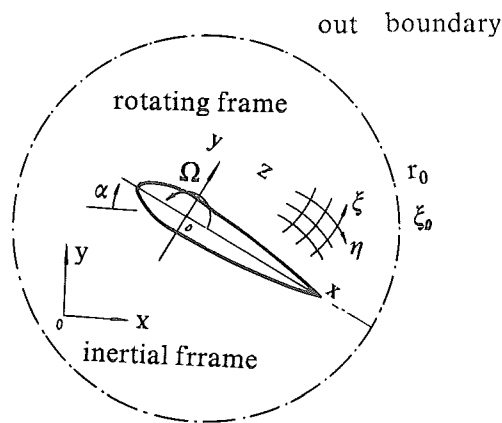
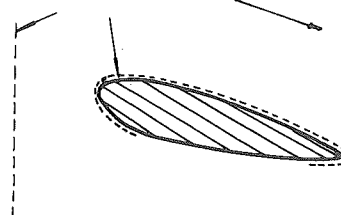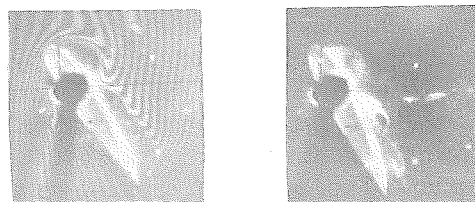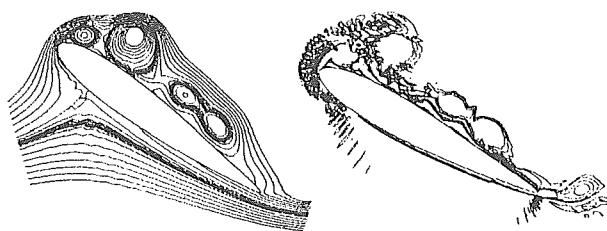Fig.1. Pitching airfoil configuration.

hydrogen bubble wire

Fig.2. A sketch of experiment set—up.

(a)　　　　　　　　(b)

(c)　　　　　　　　(d)

Fig.3. Comparitions between flow visualization picture and numerical solution. Re = 8600, $\Omega^+ = 0.24$, $x_0 / c = 0.3$, $\alpha = 50°$. (a) hydrogen bubble wire at upstream of the airfoil, (b) hydrogen bubble wire on airfoil surface, (c) calculated streemline pattern, (d) calculated vorticity field.
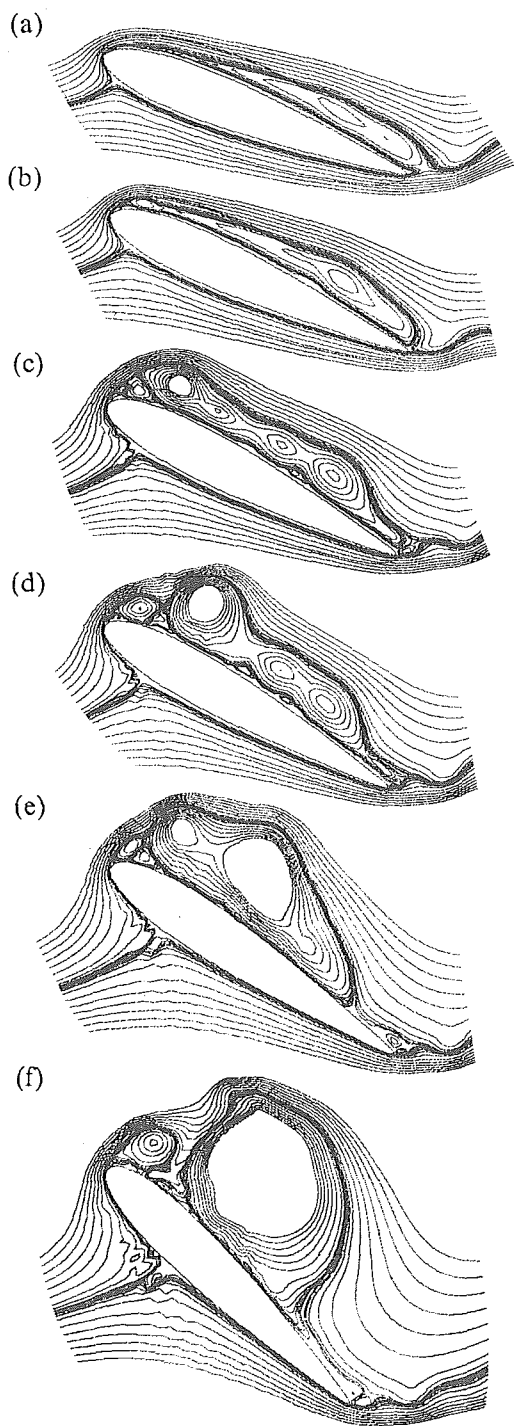
(a)

(b)

(c)

(d)

(e)

(f)

Fig.4. Flow development with time.
Re = 8600, Ω^+ = 0.24, x_0 / c = 0.3. (a) α = 30 °,
(b) α = 35 ° , (c) α = 45 ° , (d) α = 50 ° ,
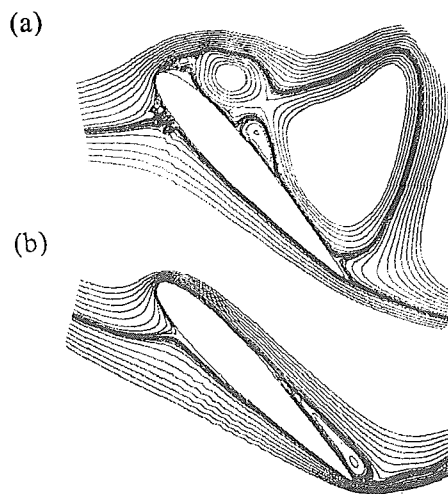(e) α = 55 ° , (f) α = 65 ° .

(a)

(b)

Fig.5. Flow field for various Ω^+.
Re = 8600, x_0 / c = 0.3. α = 45 ° .
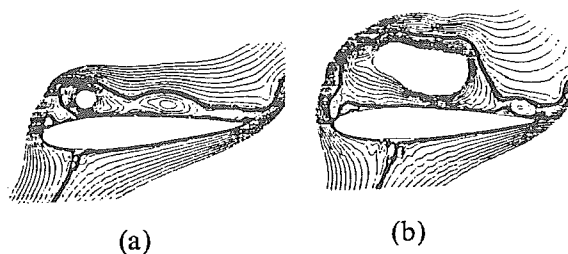(a) Ω^+ = 0.063, (b) Ω^+ = 0.64 (Ω^+ = 0.24, see fig.4c).

(a)   (b)

Fig.6. Flow   field. x_0 / c = 0.1, Re = 8600,
Ω^+ = 0.24. (a) α = 45 ° , (b) α = 60 ° .

(a)   (b)
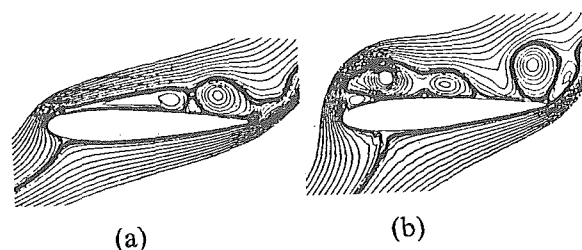
Fig.7. Flow   field. x_0 / c = 0.7, R_e = 8600,
Ω^+ = 0.24. (a) α = 45 ° , (b) α = 60 ° .

1447
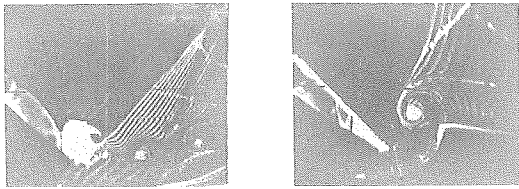
(a)   (b)

Fig.8. Structures of vortex sheet shed at trailing edge (hydrogen bubble wire on the trailing edge). (b)$\Omega^+ = 1.2$, $\alpha = 35°$, (a)$\Omega^+ = 0.17$, $\alpha = 45°$.

(a)
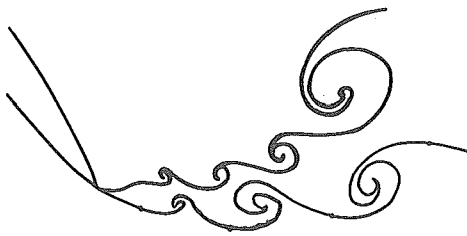
(b)

Fig.9. Structures of vortex sheet shed at trailing edge (hydrogen bubble wire on the trailing edge). ⎯⎯⎯ $\Omega^+ = 0.24$, ⎯⎯⎯ $\Omega^+ = 0.14$, (a) $\alpha = 25°$, (b) $\alpha = 45°$.
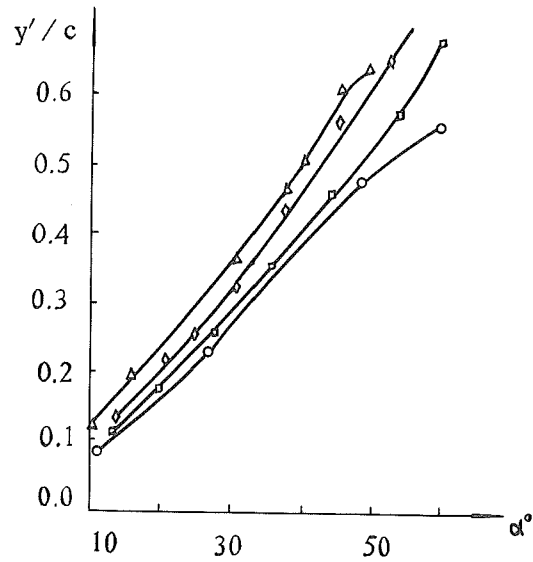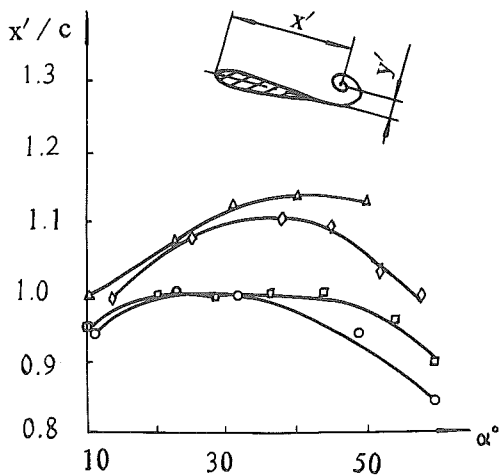

Fig.10. Locations of starting vortex.
▲ $\Omega^+ = 0.45$, ♦ $\Omega^+ = 0.64$, ▫ $\Omega^+ = 0.84$, ○ $\Omega^+ = 1.2$.
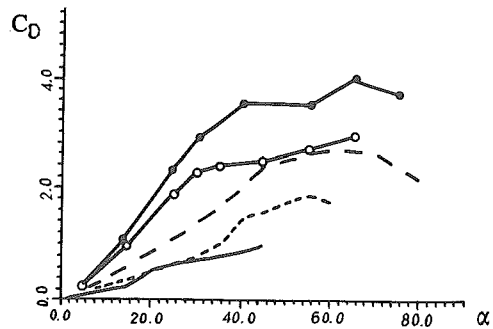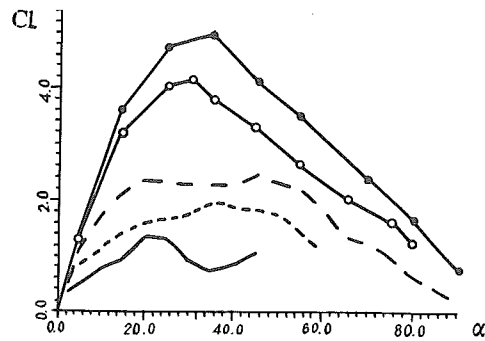

Fig.11. Lift coefficient C_L and drag coefficient C_D V.S. α. $R_e = 8600$, $x_0 / c = 0.3$ ⎯$\Omega^+ = 0.063$, ------$\Omega^+ = 0.14$, ⎯⎯$\Omega^+ = 0.24$, ♦$\Omega^+ = 0.52$, ○ $\Omega^+ = 0.64$.

1448

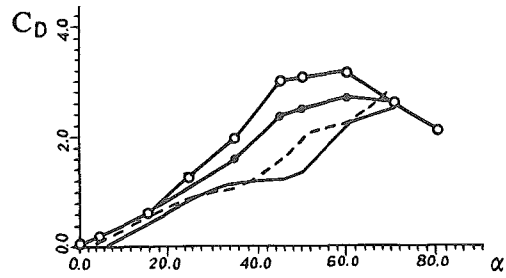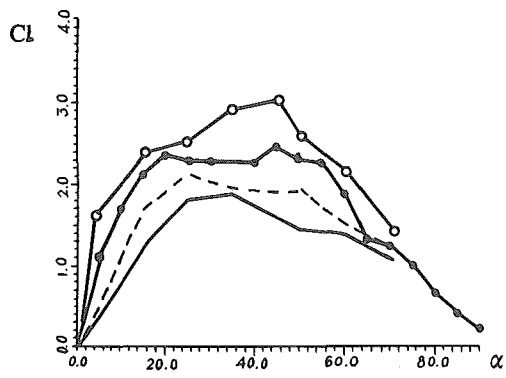Fig.12. Lift coefficient C_L and drag coefficient C_D V.S. α. Re = 8600, Ω^+ = 0.24, ——$x_0 / c = 0.7$ -----$x_0 / c = 0.5$ ... $x_0 / c = 0.3$, ... $x_0 / c = 0.1$.